TABLE III
INPUT IMPEDANCES OF AN 8-ELEMENT LOW SIDE-LOBE DIPOLE ARRAY BACKED BY A GROUND PLANE WITH AND WITHOUT A REAL SIZE TANGENTIAL OGIVE A-SANDWICH RADOME AT S BAND

els.	no radome	with radome
1	148.2+j63.3	155.1+j66.1
2	269.1+j30.7	246+j43.6
3	187.6+j64.2	191.5+j50.5
4	210.4+j57.8	219+j51.9

the radome inner surface, resulting in a strong interaction between the radome and the array. Table III presents the input impedances of the array with and without the radome. The radome effects on the input impedances of the array are clearly noted.

IV. CONCLUSIONS

The hybrid IE/PO method has been successfully used to predict the directive gain patterns and input impedance of electric dipole array in the presence of electrically large 3-D radomes. Other interesting performance indicators such as realized gain pattern and VSWR, etc, of the radome-enclosed array can also be obtained. The principal disadvantage of the technique is that discretization is required on the dielectric radome, leading to high computation complexity for larger array.

REFERENCES

[1] D. J. Kozakoff, *Analysis of Radome-Enclosed Antennas*. Norwood, MA: Artech House, 1997.

[2] J. A. Shifflett, "CADDRAD: A physical optics radar/radome analysis code for arbitrary 3D geometries," *IEEE Antennas Propag. Mag.*, vol. 39, pp. 73–79, Dec. 1997.

[3] D. T. Paris, "Computer-aided radome analysis," *IEEE Trans Antennas Propag.*, vol. AP-18, pp. 7–15, Jan. 1970.

[4] E. Arvas, A. Rahhalarabi, U. Pekel, and E. Gundogan, "Electromagnetic transmission through a small radome of arbitrary shape," *Proc. Inst. Elect. Eng.*, vol. 137, pt. H, pp. 401–405, Dec. 1990.

[5] S. M. Rao, D. R. Wilton, and A. W. Glisson, "Electromagnetic scattering by surfaces of arbitrary shape," *IEEE Trans. Antennas Propag.*, vol. AP-30, pp. 409–418, 1982.

[6] W. C. Chew, J. M. Jin, C. C. Lu, E. Michielssen, and J. M. Song, "Fast solution methods in electromagnetics," *IEEE Trans Antennas Propag.*, vol. AP-45, pp. 533–543, Mar. 1997.

[7] C. C. Lu, "A fast algorithm based on volume integral equation for analysis of arbitrarily shaped dielectric radomes," *IEEE Trans Antennas Propag.*, vol. AP-51, pp. 606–612, Mar. 2003.

[8] W. J. Zhao, L. W. Li, and Y. B. Gan, "Efficient analysis of antenna radiation in the presence of airborne dielectric radomes of arbitrary shape," *IEEE Trans Antennas Propag.*, vol. AP-53, pp. 442–449, Jan. 2005.

[9] M. A. Abdel Moneum, Z. Shen, J. L. Volakis, and O. Graham, "Hybrid PO-MoM analysis of large axi-symmetric radomes," *IEEE Trans Antennas Propag.*, vol. AP-49, pp. 1657–1666, Dec. 2001.

[10] R. S. Elliott, *Antenna Theory and Design*. New York: Wiley, 2003, p. 386.

[11] U. Jakobus and F. M. Landstorfer, "Improved PO-MM hybrid formulation for scattering from three-dimensional perfectly conducting bodies of arbitrary shape," *IEEE Trans Antennas Propag.*, vol. AP-43, pp. 162–169, Feb. 1995.

[12] U. Jakobus, "Extension of the MoM/PO hybrid technique to homogeneous dielectric bodies," in *Proc. 14th Annu. Review of Progress in Applied Computational Electromagnetics*, Monterey, Mar. 1998, vol. II, pp. 920–927, Applied Computational Electromagnetics Society.

[13] U. Jakobus and I. P. Theron, "Treatment of coated metallic surfaces with physical optics for the solution of high-frequency EMC problems," in *Proc. 15th Int. Zurich Symp. on Electromagnetic Compatibility*, Feb. 2003, pp. 257–261.

[14] U. Jakobus, "Overview of recent extensions in the electromagnetics computer code FEKO and their application," in *20th Annu. Review of Progress in Applied Computational Electromagnetics*, Syracuse, N.Y., Apr. 2004, Applied Computational Electromagnetics Society.

[15] P. L. Overfelt, "Superspheroids: A new family of radome shapes," *IEEE Trans. Antennas Propag.*, vol. AP-43, no. 2, pp. 215–220, 1995.

[16] R. W. McMillan, M. C. Wicks, and G. J. Genello, "A model for determination of radome transmission, reflection, depolarization, loss, and effects on antenna patterns," in *Proc. IEEE Radar Conf.*, Dallas, TX, 1998, pp. 349–354.

Passive Localization of Near-Field Sources With a Polarization Sensitive Array

Yuntao Wu, H. C. So, Chaohuan Hou, and Jun Li

***Abstract*—The least squares-virtual ESPRIT algorithm (LS-VESPA) is extended to jointly estimate the direction-of-arrival (DOA) and ranges of multiple near-field sources impinging on an array of crossed dipoles. The algorithm utilizes fourth-order cumulants for direct estimation of the arrival angle and range parameters via the eigenvalues of certain constructed matrices. Compared with several existing algorithms, the loss of array aperture is effectively avoided. As a result, the proposed method can estimate DOAs and ranges of $(N-1)$ polarized near-field sources using N dual-polarization sensors. Simulation results show that the proposed method outperforms a fourth-order statistics based ESPRIT-like method.**

***Index Terms*—Least squares-virtual ESPRIT algorithm (LS-VESPA), near-field, polarization, source localization.**

I. INTRODUCTION

Many methods for estimation of directions of arrival (DOAs) of emitted sources impinging on an array of sensors have been developed in the field of array signal processing [1], such as multiple signal classification (MUSIC) and estimation of signal parameters via rotational invariance techniques (ESPRIT). Most of them assume that the sources of interest are located relatively far from the array so that the wavefronts from them can be regarded as plane waves, which implies that each source location is characterized by a single DOA [1]. Apparently, this assumption is no longer valid when the source is close to the array, such as in near-field applications of sonar [2], seismic exploration [3], and electronic surveillance [4]. For near-field sources, they must be characterized by spherical wavefronts at the array aperture and need to be localized by both range and DOA [2]–[5].

Since the available methods based on the far-field assumption cannot be directly applied to the near-field scenario, near-field source localization is typically solved by other means, such as maximum likelihood (ML) [2], multidimensional search [4], 2D-MUSIC [5]–[9], and higher order statistics [10]. To avoid the multidimensional search, Challa and Shamsunder [10], [11] have developed a total least squares ESPRIT-like algorithm as well as unitary ESPRIT method based on fourth-order cumulants. An optimally-weighted linear prediction method for near-field source localization is also recently presented in [12], where

Manuscript received August 14, 2006; revised December 20, 2006.

Y. Wu and H. C. So are with the Department of Electronic Engineering, City University of Hong Kong, Kowloon, Hong Kong (e-mail: wuyuntao6@hotmail.com).

C. Hou is with the Integrated Digital System Laboratory, Institute of Acoustics, Chinese Academy of Sciences, Beijing, 100080, China.

J. Li is with the National Key Laboratory for Radar Signal Processing, Xidian University, Xian, 710071, China.

Color versions of one or more of the figures in this paper are available online at http://ieeexplore.ieee.org.

Digital Object Identifier 10.1109/TAP.2007.901912

multiple optimally weighted least squares problems need to be firstly solved for parameter estimation.

All aforementioned methods for near-field source localization do not exploit the polarization information at the received array. Nevertheless, the advantages of different polarization-sensitive arrays have been utilized in wireless communications and various types of radar systems [14], [16]. The problem of parameter estimation of far-field signal source with a diversely polarized array has been extensively studied [14]–[16]. This is motivated by the fact that polarization has also been incorporated in array antennas for improved estimation of far-field signal parameters. Recently, an enhanced method for near-field source localization with a polarization sensitive array has been presented in [17], which shows that the incorporation of the source polarization information can provide improved performance over the case of ignoring the available polarization information. Although direct estimation of the DOA and range parameters can be performed in a computationally attractive manner using the methods of [10]–[12], [17], they need to exploit the symmetric structure of the sensor position coordinate system. As a result, the effective aperture of array is reduced by half. In order to enhance the estimation performance and increase the resolution accuracy particularly for closely-spaced sources, more sensors and larger array aperture are required. This implies the need of more complex system hardware and increased computation burden.

The goal of this paper is to reduce the loss of the array aperture in conventional ESPRIT-like methods for localization of near-field sources, and then obtain the performance improvement of resolving closely spaced signals with a small number of sensors. By using the cumulant-based matrices instead of those used in the conventional ESPRIT-like methods [17], a uniform linear array with N dual-polarization sensors can be used to resolve DOAs of up to $(N-1)$ signals, which is twice the maximum number of DOAs that can be estimated by several available methods [10]–[12], [17]. In fact, this paper can also be regarded as an extension of the least squares-virtual ESPRIT algorithm (LS-VESPA) proposed in [19] to the problem of near-field source localization.

This paper is organized as follows. Section II describes the data model of near-field source localization with a polarization sensitive array and the problem formulation. Section III shows how the LS-VESPA can be utilized to estimate the two dimensional parameters of near-field sources. Finally, simulation results are provided in Section IV, followed by a conclusion in Section V.

II. Problem Formulation

Consider P near-field narrow-band sources impinging on a uniform linear array of N dual-polarization sensors with inter-element spacing d. The array configuration is shown in Fig. 1, where all the sensors, namely, $-1, 0, \ldots, N-2$, lie on the y-axis. The pair of variables (θ_i, r_i) denotes the DOA and range of source i at the reference sensor 0.

Given a transverse electromagnetic (TEM) wave propagating into the array, we consider the polarization ellipse produced by its electric field as the incoming wave is viewed from the coordinate origin.

Suppose the electric field has transverse components

$$\vec{\mathbf{E}} = E_\phi \vec{\boldsymbol{\phi}} + E_\theta \vec{\boldsymbol{\theta}} \tag{1}$$

where $E_{\boldsymbol{\phi}}$ is the horizontal component and $E_{\boldsymbol{\theta}}$ is the vertical component, and $\vec{\boldsymbol{\phi}}$ and $\vec{\boldsymbol{\theta}}$ are the spherical unit vectors along the azimuth and elevation angles ϕ and θ, respectively. For simplicity, it is assumed that the source signal is in the $y-z$ plane perpendicular to that of the array which is located in the $x-y$ plane. Then, $\phi = 90^\circ$, $\vec{\boldsymbol{\phi}} = -\vec{\mathbf{x}}$ and

$$\vec{\mathbf{E}} = -E_\phi \vec{\mathbf{x}} + E_\theta \vec{\boldsymbol{\theta}} = -E_\phi \vec{\mathbf{x}} + E_\theta \cos(\theta)\vec{\mathbf{y}} - E_\theta \sin(\theta)\vec{\mathbf{z}} \tag{2}$$

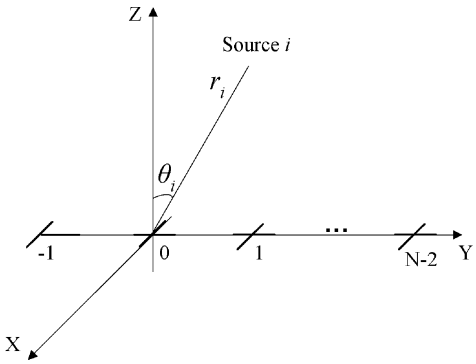

Fig. 1. Uniformly spaced linear array configuration.

with $\vec{\mathbf{x}}$, $\vec{\mathbf{y}}$ and $\vec{\mathbf{z}}$ representing the unit vectors along the x, y and z directions, respectively. Alternatively, the polarized signal can be described as

$$\begin{bmatrix} E_\phi \\ E_\theta \end{bmatrix} = \begin{bmatrix} E_0 \cos(\gamma) \\ E_0 \sin(\gamma) e^{j\beta} \end{bmatrix} \tag{3}$$

where γ and β denote the magnitude ratio and the phase between the two polarization components, and E_0 represents the signal amplitude which is an arbitrary nonzero complex constant.

With the use of (3), (2) can be written as

$$\vec{\mathbf{E}} = E_0(-\cos(\gamma)\vec{\mathbf{x}} + \cos(\theta)\sin(\gamma)e^{j\beta}\vec{\mathbf{y}} - \sin(\theta)\sin(\gamma)e^{j\beta}\vec{\mathbf{z}}). \tag{4}$$

The signal component in the $\vec{\mathbf{z}}$ direction is eliminated using the specific orientation of the cross-polarized array of Fig. 1. Apparently, the value of θ in (4) varies at each of the N sensors. It is straightforward to show that the DOA of the ith source signal at sensor m, denoted by θ_{mi}, is

$$\theta_{mi} = \sin^{-1}\left(\frac{r_i \sin(\theta_i) - md}{\sqrt{r_i^2 + m^2 d^2 - 2r_i md\sin(\theta_i)}}\right). \tag{5}$$

The received signals at sensor m for polarization x and y, denoted by $u_m^{[x]}(t)$ and $u_m^{[y]}(t)$, can be approximated as [17]

$$u_m^{[x]}(t) = -\sum_{i=1}^{P} s_i(t)\cos(\gamma_i)e^{j(\omega_i m + \phi_i m^2)} + n_m^{[x]}(t)$$

and

$$u_m^{[y]}(t) = \sum_{i=1}^{P} s_i(t)\cos(\theta_{mi})\sin(\gamma_i)e^{j\beta_i}e^{j(\omega_i m + \phi_i m^2)} + n_m^{[y]}(t) \qquad m = -1, 0, 1, \ldots, N-2 \tag{6}$$

where $n_m^{[l]}(t), l = x,\ y$, is the noise component for polarization l at the mth sensor and s_i is the ith source signal. The parameters ω_i and ϕ_i are functions of the azimuth angle θ_i and range r_i of the ith source, and they are related as

$$\omega_i = \frac{-2\pi}{\lambda} d\sin(\theta_i) \qquad \text{and} \qquad \phi_i = \pi\frac{d^2}{\lambda r_i}\cos^2(\theta_i) \tag{7}$$

where λ denotes the wavelength of the source wavefronts. The task is to estimate the parameters $\{\theta_1, \ldots, \theta_P, r_1, \ldots, r_P\}$ of the P sources from the received array data $\{u_{-1}^l(t), \ldots, u_{N-2}^l(t)\}, l = x,\ y$.

For unique parameter estimation, we have made the following assumptions.

(A1) The P sources $\{s_1(t), \ldots, s_P(t)\}$ are assumed to be zero mean, statistically independent of each other and have nonzero fourth-order cumulants, whereas the additive noise components

TABLE I
COMPARISON OF DIFFERENT ALGORITHMS FOR N DOAS ESTIMATION

Algorithm	Minimum number of sensors	Search required	Initialization required	Pairing required
2-D MUSIC[5,6,7,9]	$N+1$	Yes	Yes	No
ESPRIT-like[10,17]	$2N$	No	No	Yes
WLP method[12]	$2N+1$	No(iteration required)	No	Yes
Proposed algorithm	$N+1$	No	No	Yes

Remark: the proposed method for estimation of N signal sources needs only $N+1$ sensors, but other methods without $2D$ search computation need a minimum of $2N$ sensors.

$n_m^{[x]}(t)$ and $n_m^{[y]}(t)$ are zero mean, Gaussian distributed and independent of the source signals.

(A2) The inter-element spacing between two adjacent dipole pairs d satisfies $d \leq \lambda/4$ to avoid ambiguity problem of angle estimation. It is noteworthy that in [10], [11], the use of cumulants to linearize the quadratic phase in (6) renders the near-field sources to be equivalent to multiple far-field sources observed with a virtual array of sensors spaced $2d$ apart. As a result, (A2) is required so that the effective sensor spacing is again $\lambda/2$ as dictated by the spatial Nyquist criterion.

(A3) The number of required sensors is $N > P$, whose minimum is around half of those in [10], [12], [17]. Table I shows a requirement comparison of different DOA estimation algorithms.

In practice, there is mutual coupling between the array elements. Since effective methods have already been introduced to compensate the coupling effect in the ESPRIT direction finding algorithm [20], [21], we can employ them to pre-process the received array data or for pre-calibration. As a result, we assume that the mutual coupling effect has been removed in advance. Furthermore, both the sensor position errors as well as gain and phase errors of all sensors are assumed to be negligible.

From (6), the array outputs can be written in matrix form as

$$\mathbf{u}^{[l]}(t) = \mathbf{A}^{[l]}\mathbf{s}^{[l]}(t) + \mathbf{n}^{[l]}(t), \quad l = x, y \tag{8}$$

where

$$\begin{aligned}
\mathbf{u}^{[l]}(t) &= [u_{-1}^{[l]} \quad u_0^{[l]} \quad u_1^{[l]} \quad \cdots \quad u_{N-2}^{[l]}]^T \\
\mathbf{s}^{[x]}(t) &= -[s_1(t)\cos(\gamma_1), \quad \cdots \quad s_P(t)\cos(\gamma_P)]^T \\
\mathbf{s}^{[y]}(t) &= [s_1(t)\sin(\gamma_1)e^{j\beta_1}, \quad \cdots \quad s_P(t)\sin(\gamma_P)e^{j\beta_P}]^T
\end{aligned}$$

and

$$\mathbf{n}^{[l]} = [n_{-1}^{[l]} \quad n_0^{[l]} \quad \cdots \quad n_{N-2}^{[l]}]^T, \quad l = x, y$$

where T denotes transpose. The columns of the polarization-dependent $N \times P$ steering matrices $\mathbf{A}^{[x]}$ and $\mathbf{A}^{[y]}$ are

$$\begin{aligned}
&\mathbf{a}_i^{[x]}(\theta_i, r_i) \\
&\quad = [e^{j(-1)\omega_i + j(-1)^2\phi_i} \; 1 \; e^{j(\omega_i+\phi_i)} \cdots e^{j(N-2)\omega_i + j(N-2)^2\phi_i}]^T \\
&\mathbf{A}^{[x]} = [\mathbf{a}_1, \ldots, \mathbf{a}_P] \\
&\mathbf{a}_i^{[y]}(\theta_i, r_i) \\
&\quad = [e^{j(-1)\omega_i + j(-1)^2\phi_i}\cos(\theta_{-1i}) \quad \cos(\theta_{0i}), \ldots, \\
&\qquad e^{j(N-2)\omega_i + j(N-2)^2\phi_i}\cos(\theta_{(N-2)i})]^T
\end{aligned}$$

and

$$\mathbf{A}^{[y]} = [\mathbf{a}_1^{[y]}, \ldots, \mathbf{a}_P^{[y]}].$$

Note that the source polarization appears in both $\mathbf{s}^{[l]}(t)$ and $\mathbf{A}^{[y]}$.

III. THE PROPOSED ALGORITHM

Due to the quadratic dependence of signal phase on sensor location in (6), far-field source localization methods cannot be directly applied to the case of near-field sources. Our key idea is to explore the possibility to reduce the polynomial order of the exponent in (6), so that existing algorithms based on far-field assumption can be utilized. Since second-order correlations have only one lag, it is not possible to achieve the polynomial order reduction. On the other hand, cumulants with multiple lags can provide the desired extra degrees of freedom. In this work, cumulant matrices generated from (9) will be used for the development of the near-field source localization algorithm. Since the available dual-polarization is exploited, it is expected that the developed algorithm will yield better estimation performance than those without utilizing it.

We first define the fourth-order cumulant of the complex measurements of $\{u_0^{[l]}(t), u_0^{[l]*}(t), u_k^{[l]}(t), u_h^{[l]*}(t)\}$, where "*" represents the complex conjugate, which is denoted as cum $(u_0^{[l]}(t), u_0^{[l]*}(t), u_k^{[l]}(t), u_h^{[l]*}(t))$. From (6) and the cumulant properties in [18], it follows that:

$$\begin{aligned}
&\mathrm{cum}(u_0^{[l]}(t), u_0^{[l]*}(t), u_k^{[l]}(t), u_h^{[l]*}(t)) \\
&\qquad = \sum_{i=1}^{P} c_{4,s_i^{[l]}} e^{j(k-h)\omega_i + j(k^2-h^2)\phi_i}
\end{aligned} \tag{9}$$

where $c_{4,s_i}^{[l]}$, $i = 1, 2, \ldots, P$, denotes the kurtosis of the ith signal source for polarization l and is defined as

$$c_{4,s_i}^{[l]} = \mathrm{cum}\{s_i^{*[l]}(t), s_i^{[l]}(t), s_i^{*[l]}(t), s_i^{[l]}(t)\} = E\{|s_i^{[l]}(t)|^4\} - 2E^2\{|s_i^{[l]}(t)|^2\} \tag{10}$$

where E denotes the expectation operator and $s_i^{[l]}(t)$ is the ith element in $\mathbf{s}^{[l]}(t)$. According to the independence of the source signals in (A1), we have

$$\begin{aligned}
&\mathrm{cum}(s_{k_1}^{[l]}(t), s_{k_2}^{[l]*}(t), s_{k_3}^{[l]}(t), s_{k_4}^{[l]*}(t)) \\
&\qquad = \begin{cases} c_{4,s_k^{[l]}}, & \text{if } k_1 = k_2 = k_3 = k_4 \\ 0, & \text{otherwise.} \end{cases}
\end{aligned} \tag{11}$$

A. Extended LS-VESPA Derivation

In order to obtain the required rotational matrix in our proposed algorithm, we assign the sensor $m = 0$ as the phase reference point which is different from the center-symmetric array requirement in [17]. Compared to the ESPRIT-like method [17], three constant guiding sensors, namely, -1, 0 and 1, are exploited to construct the required cumulant matrices in the LS-VESPA.

For $k, h = -1, \ldots, N-2$, the auto-polarized cumulant matrix is obtained as

$$\begin{aligned}
\mathbf{C}_0^{[ll]} &\triangleq \mathrm{cum}(u_0^{[l]}(t), u_0^{[l]*}(t), \mathbf{u}^{[l]}(t), \mathbf{u}^{[l]H}(t)) \\
&= \mathbf{A}^{[l]}\mathbf{C}_{4s}^{[ll]}\mathbf{A}^{[l]H}, \quad l = x, y.
\end{aligned} \tag{12}$$

Using (11) and different polarizations, we get the cross-polarized and auto-polarized kurtosis of the kth signal

$$\mathbf{C}_{4s}^{[xx]} = \mathbf{P}\mathbf{C}_{4s}\mathbf{P} \quad \mathbf{C}_{4s}^{[xy]} = \mathbf{P}\mathbf{C}_{4s}\mathbf{Q} \text{ and } \mathbf{C}_{4s}^{[yy]} = \mathbf{Q}\mathbf{C}_{4s}\mathbf{Q} \quad (13)$$

where $\mathbf{P} = \text{diag}(\cos^2(\gamma_1), \ldots, \cos^2(\gamma_N))$, $\mathbf{Q} = \text{diag}(\sin^2(\gamma_1), \ldots, \sin^2(\gamma_N))$ and $\mathbf{C}_{4s} = \text{diag}(c_{4s_1}, \ldots, c_{4s_P})$.

Similarly, with the use of different sensor lags, we construct the following cumulant matrices $\mathbf{C}_1^{[ll]}$ and $\mathbf{C}_2^{[ll]}$, $l = x, y$

$$\begin{aligned}\mathbf{C}_1^{[ll]} &\triangleq \text{cum}(u_0^{[l]}(t), u_{-1}^{[l]*}(t), \mathbf{u}^{[l]}(t), \mathbf{u}^{[l]H}(t)) \\ &= \mathbf{A}^{[l]}\mathbf{\Phi}_1\mathbf{C}_{4s}^{[ll]}\mathbf{A}^{[l]H} \end{aligned} \quad (14)$$

and

$$\begin{aligned}\mathbf{C}_2^{[ll]} &\triangleq \text{cum}(u_1^{[l]}(t), u_{-1}^{[l]*}(t), \mathbf{u}^{[l]}(t), \\ \mathbf{u}^{[l]H}(t)) &= \mathbf{A}^{[l]}\mathbf{\Phi}_2\mathbf{C}_{4s}^{[ll]}\mathbf{A}^{[l]H} \end{aligned} \quad (15)$$

where $\mathbf{\Phi}_1 = \text{diag}(e^{j(\omega_1-\phi_1)}, \ldots, e^{j(\omega_P-\phi_P)})$, $\mathbf{\Phi}_2 = \text{diag}(e^{j2\omega_1}, \ldots, e^{j2\omega_P})$ and H stands for Hermitian transposition.

We further define the following cross-polarized cumulant matrices:

$$\begin{aligned}\mathbf{C}_0^{[lq]} &\triangleq \text{cum}(u_0^{[l]}(t), u_0^{[q]*}(t), \mathbf{u}^{[l]}(t), \mathbf{u}^{[q]H}(t)) \\ &= \mathbf{A}^{[l]}\mathbf{C}_{4s}^{[lq]}\mathbf{A}^{[q]H} \end{aligned} \quad (16)$$

$$\begin{aligned}\mathbf{C}_1^{[lq]} &\triangleq \text{cum}(u_0^{[l]}(t), u_{-1}^{[q]*}(t), \mathbf{u}^{[l]}(t), \mathbf{u}^{[q]H}(t)) \\ &= \mathbf{A}^{[l]}\mathbf{\Phi}_1\mathbf{C}_{4s}^{[lq]}\mathbf{A}^{[q]H} \end{aligned} \quad (17)$$

and

$$\begin{aligned}\mathbf{C}_2^{[lq]} &\triangleq \text{cum}(u_1^{[l]}(t), u_{-1}^{[q]*}(t), \mathbf{u}^{[l]}(t), \mathbf{u}^{[q]H}(t)) \\ &= \mathbf{A}^{[l]}\mathbf{\Phi}_2\mathbf{C}_{4s}^{[lq]}\mathbf{A}^{[q]H}. \end{aligned} \quad (18)$$

The first two elements in $\mathbf{C}_0^{[lq]}$, $\mathbf{C}_1^{[lq]}$, and $\mathbf{C}_2^{[lq]}$, $l, q = x, y$, namely, $u_{-1}^{[l]}$, $u_0^{[l]}$, and $u_1^{[l]}$, are guiding sensors for constructing $\mathbf{C}_0^{[lq]}$, $\mathbf{C}_1^{[lq]}$, and $\mathbf{C}_2^{[lq]}$, respectively. The sensor $m = 0$ is set to be the phase reference point in our method while the phase reference point must locate at the symmetry center of array in [10], [12], [17]. We exploit efficiently the symmetry of sensor pair $\{u_{-1}^{[l]}, u_1^{[l]}\}$, $l = x, y$, to construct the cumulant matrix $\mathbf{C}_2^{[lq]}$ and then yield the rotational matrix $\mathbf{\Phi}_2$ which is a function of $\{\omega_i\}$ only. This also suggests the important usage of symmetry of sensor pair $\{u_{-1}^{[l]}, u_1^{[l]}\}$, $l = x, y$, is to eliminate the quadratic phase ϕ_i of the signal model of (6) by cumulant computation. Assuming that the steering matrix $\mathbf{A}^{[l]}$, $l = x, y$, and $\mathbf{C}_s^{[lq]}$, $l, q = x, y$, are of full rank, (12)–(18) satisfy all the requirements of the LS-VESPA .

Combining the cumulant matrices $\mathbf{C}_0^{[lq]}$, $\mathbf{C}_1^{[lq]}$, and $\mathbf{C}_2^{[lq]}$, $l, q = x, y$, we form four $3N \times N$ matrices

$$\mathbf{C}_c^{[lq]} = \begin{bmatrix} \mathbf{C}_0^{[lq]} \\ \mathbf{C}_1^{[lq]} \\ \mathbf{C}_2^{[lq]} \end{bmatrix}, \quad l, q = x, y. \quad (19)$$

Now applying the LS-VESPA method and we easily obtain the dual-polarized matrix

$$\mathbf{C} = \begin{bmatrix} \mathbf{C}_c^{[xx]} & \mathbf{C}_c^{[xy]} \\ \mathbf{C}_c^{[yx]} & \mathbf{C}_c^{[yy]} \end{bmatrix} = \begin{bmatrix} \tilde{\mathbf{A}}^{[x]} \\ \tilde{\mathbf{A}}^{[y]} \end{bmatrix} \mathbf{C}_{4s}[\mathbf{A}^{[x]}\mathbf{P} \quad \mathbf{A}^{[y]}\mathbf{Q}]^H \quad (20)$$

where

$$\tilde{\mathbf{A}}^{[x]} = \begin{bmatrix} \mathbf{A}^{[x]}\mathbf{P} \\ \mathbf{A}^{[x]}\mathbf{P}\mathbf{\Phi}_1 \\ \mathbf{A}^{[x]}\mathbf{P}\mathbf{\Phi}_2 \end{bmatrix} \quad \text{and} \quad \tilde{\mathbf{A}}^{[y]} = \begin{bmatrix} \mathbf{A}^{[y]}\mathbf{Q} \\ \mathbf{A}^{[y]}\mathbf{Q}\mathbf{\Phi}_1 \\ \mathbf{A}^{[y]}\mathbf{Q}\mathbf{\Phi}_2 \end{bmatrix}. \quad (21)$$

From (20), it is evident that the polarization diversity doubles the space dimension of the conventional problem formulation without polarization information.

Using the idea of the ESPRIT algorithm, the signal subspace $\mathbf{E}_s$ of the matrix $\mathbf{C}$ can be obtained by the P eigenvectors of the cumulant matrix $\mathbf{C}$ corresponding to the P nonzero eigenvalues

$$\begin{aligned}\mathbf{E}_s &= \{\mathbf{e}_1, \ldots, \mathbf{e}_P\} \\ &= \begin{bmatrix} (\mathbf{E}_0^{[x]})^T & (\mathbf{E}_1^{[x]})^T & (\mathbf{E}_2^{[x]})^T & (\mathbf{E}_0^{[y]})^T & (\mathbf{E}_1^{[y]})^T & (\mathbf{E}_2^{[y]})^T \end{bmatrix}^T \\ &= [(\tilde{\mathbf{A}}^{[x]})^T \quad (\tilde{\mathbf{A}}^{[y]})^T]^T\mathbf{F} \end{aligned} \quad (22)$$

where $\mathbf{F}_{P\times P}$ is an invertible matrix.

Combining the definitions of $\tilde{\mathbf{A}}^{[x]}$ and $\tilde{\mathbf{A}}^{[y]}$ and using the rotational invariance of subspace, we obtain

$$[(\mathbf{E}_1^{[x]})^T \quad (\mathbf{E}_1^{[y]})^T]^T = [(\mathbf{E}_0^{[x]})^T \quad (\mathbf{E}_0^{[y]})^T]^T\mathbf{\Psi}_1 \quad (23)$$

and

$$[(\mathbf{E}_2^{[x]})^T \quad (\mathbf{E}_2^{[y]})^T]^T = [(\mathbf{E}_0^{[x]})^T \quad (\mathbf{E}_0^{[y]})^T]^T\mathbf{\Psi}_2. \quad (24)$$

Furthermore, $\mathbf{\Psi}_1$ and $\mathbf{\Psi}_2$ can be computed by using least-squares

$$\begin{aligned}\mathbf{\Psi}_1 &= ([(\mathbf{E}_0^{[x]})^T \quad (\mathbf{E}_0^{[y]})^T]^T)^{\#}[(\mathbf{E}_1^{[x]})^T \quad (\mathbf{E}_1^{[y]})^T]^T \quad \text{and} \\ \mathbf{\Psi}_2 &= ([(\mathbf{E}_0^{[x]})^T \quad (\mathbf{E}_0^{[y]})^T]^T)^{\#}[(\mathbf{E}_2^{[x]})^T \quad (\mathbf{E}_2^{[y]})^T]^T \end{aligned} \quad (25)$$

where $\#$ denotes the pseudo-inverse of a matrix.

According to (21) and (22), we have

$$\mathbf{\Psi}_1 = \mathbf{F}_1^{-1}\mathbf{\Phi}_1\mathbf{F}_1 \quad \text{and} \quad \mathbf{\Psi}_2 = \mathbf{F}_2^{-1}\mathbf{\Phi}_2\mathbf{F}_2 \quad (26)$$

where the columns of $\mathbf{F}_1$ and $\mathbf{F}_2$ are the eigenvectors of $\mathbf{\Psi}_1$ and $\mathbf{\Psi}_2$, respectively. Hence the eigenvalues of $\mathbf{\Psi}_1$ and $\mathbf{\Psi}_2$ give the estimates of the diagonal elements of $\mathbf{\Phi}_1$ and $\mathbf{\Phi}_2$, respectively.

Since the independent eigendecompositions of $\mathbf{\Psi}_1$ and $\mathbf{\Psi}_2$ lead to arbitrary ordering of the diagonal elements in $\mathbf{\Phi}_1$ and $\mathbf{\Phi}_2$, we first need to pair the elements of the two sets of parameters $\{\omega_i - \phi_i\}$, $\{2\omega_i\}$. Fortunately, the eigenvalues of $\mathbf{\Psi}_1$ and $\mathbf{\Psi}_2$ correspond to the same eigenvector of $\mathbf{F}$ in (22), which can then be used to restore the correct parameter pairs.

In fact, pairing of $\mathbf{\Phi}_1$ and $\mathbf{\Phi}_2$ is equivalent to pairing of the eigenvectors of $\mathbf{\Psi}_1$ and $\mathbf{\Psi}_2$. Here we repeat the same pairing procedure of Liu and Mendel in [19]. The procedure is based on projecting the columns of $\mathbf{F}_1$ onto eigenspaces of $\mathbf{\Psi}_2$. Let $\mathbf{f}_{1k}$, $k = 1, 2, \ldots, P$, be the k-th column of $\mathbf{F}_1$, then each entry in the complex projection row vector $\mathbf{f}_{1k}^H\mathbf{F}_2$ represents the eigenspaces will have their magnitudes less than unity since we are in the complex domain. In the presence of noise, we pick $\mathbf{f}_{2l}$, $l \in \{1, 2, \ldots, P\}$, such that the magnitude of $\mathbf{f}_{1k}^H\mathbf{f}_{2l}$ is closest to unity. Next, we form the eigenvalue pair $\{\mathbf{\Phi}_1(k,k), \mathbf{\Phi}_2(l,l)\}$, $k, l = 1, 2, \ldots, P$, where their associated eigenvectors are $\mathbf{f}_{1k}$ and $\mathbf{f}_{2l}$ from $\mathbf{F}_1$ and $\mathbf{F}_2$, respectively.

From each pair of $(\hat{\omega}_i, \hat{\phi}_i)$, $i = 1, 2, \ldots, P$, the DOA and range parameters are computed as

$$\hat{\theta}_i = \sin^{-1}\left(\frac{-\lambda\hat{\omega}_i}{2\pi d}\right) \quad (27)$$

and

$$\hat{r}_i = \frac{\pi d^2\cos^2(\hat{\theta}_i)}{\lambda\hat{\phi}_i}. \quad (28)$$

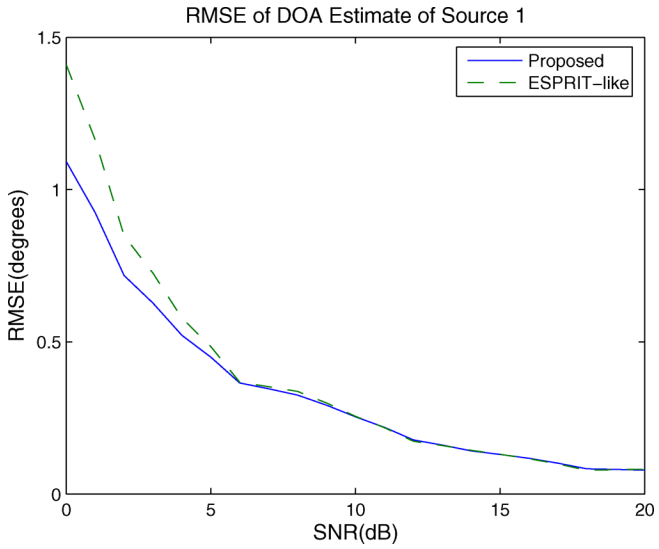

Fig. 2. The RMSE of estimated DOA for source 1 versus input SNR. The parameters of two sources are $(40^\circ, 5\lambda; 20^\circ, 3.5\lambda)$. There are four sensors and 1000 snapshots are used.

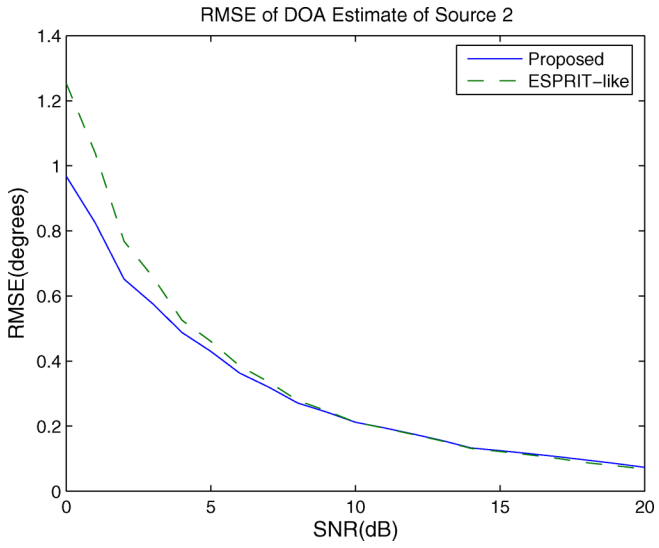

Fig. 3. The RMSE of estimated DOA for source 2 versus input SNR. The parameters of two sources are $(40^\circ, 5\lambda; 20^\circ, 3.5\lambda)$. There are four sensors and 1000 snapshots are used.

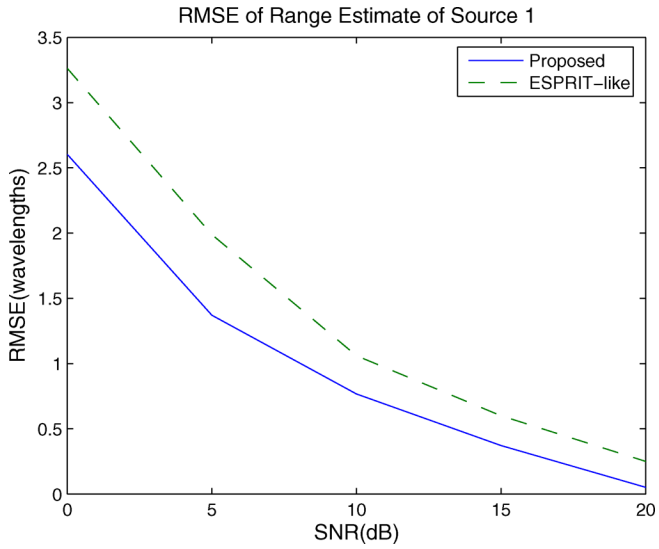

Fig. 4. The RMSE of estimated range for source 1 versus input SNR. The parameters of two sources are $(40^\circ, 5\lambda; 20^\circ, 3.5\lambda)$. There are four sensors and 1000 snapshots are used.

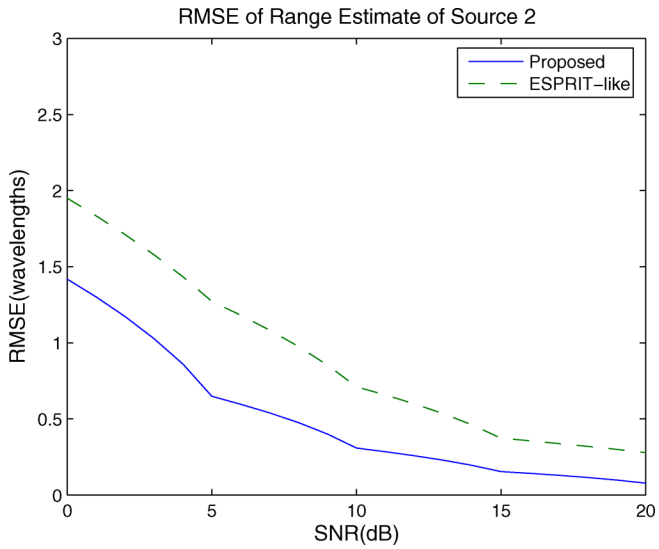

Fig. 5. The RMSE of estimated range for source 2 versus input SNR. The parameters of two sources are $(40^\circ, 5\lambda; 20^\circ, 3.5\lambda)$. There are four sensors and 1000 snapshots are used.

The procedure of our proposed algorithm is summarized as follows:

- Compute $\mathbf{C}_0^{[lq]}$, $\mathbf{C}_1^{[lq]}$, and $\mathbf{C}_2^{[lq]}$, $l, q = x, y$, defined in (12)–(18);
- Perform singular value decomposition (SVD) of $\mathbf{C}$ to estimate the number of incident signals P using the well-known minimum description length (MDL) criterion [22] and then obtain the $\mathbf{E}_s$ in (22);
- Compute the $\mathbf{\Psi}_1$ and $\mathbf{\Psi}_2$ using (25).
- Eigendecompose $\mathbf{\Psi}_1$ and $\mathbf{\Psi}_2$ to obtain $\mathbf{\Phi}_1, \mathbf{F}_1, \mathbf{\Phi}_2$, and $\mathbf{F}_2$;
- Align $\mathbf{\Phi}_1(i,i)$ and $\mathbf{\Phi}_2(i,i), i = 1, \ldots, P$ and obtain the estimates of ω_i and ϕ_i;
- Compute $\hat{\theta}_i$ and $\hat{r}_i, i = 1, 2, \ldots, P$ using (27) and (28).

IV. Simulation Results

To verify the performance of the proposed method, a set of computer simulations is carried out. We consider a uniform linear array consisting of several crossed dipoles with the inter-spacing $d = \lambda/4$. The reference sensor is sensor 0. Two equal power uncorrelated TEM waves with non-Gaussian distribution are impinging on this array and are modelled as $e^{j\phi_t}$, where the phases ϕ_t are uniformly distributed in the interval $[0, 2\pi]$. The sensor noise is additive Gaussian process. The estimation performance is measured by the root mean square error (RMSE). The RMSE of range parameter is normalized by the signal wavelength λ. The polarization parameters (γ, β) of the two sources are $(10^\circ, 0^\circ)$ and $(80^\circ, 0^\circ)$.

In the first experiment, the first source is located at $\theta_1 = 40^\circ$ with a range of $r_1 = 5\lambda$ while the second source is located at $\theta_2 = 20^\circ$ with a range of $r_2 = 3.5\lambda$. The number of sensors is $N = 4$ and the number of samples at each sensor is $T = 1000$. All provided results are averages of 100 independent runs. The results for range and DOA estimates of the two sources are shown in Figs. 2–5. For comparison, the results using the ESPRIT-like algorithm [17] are also shown. Figs. 2 and 3 show that the proposed method outperforms the ESPRIT algorithm in

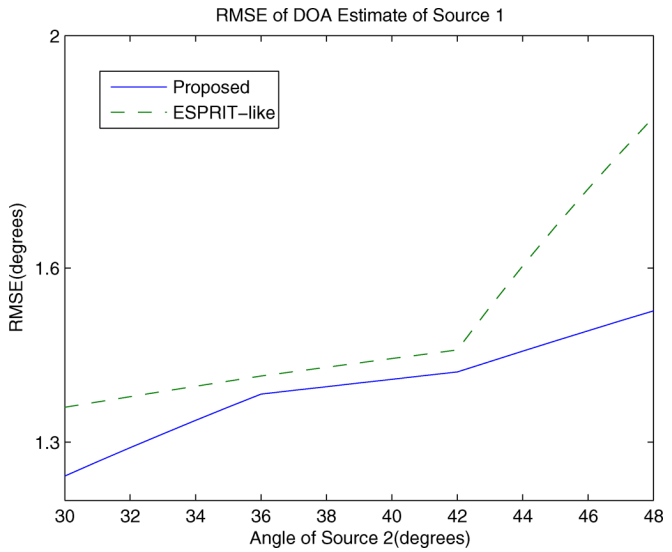

Fig. 6. The RMSE of estimated DOA for source 1 plotted as a function of the DOA of source 2. The DOA of source 1 is fixed at 50° and there are four sensors. The ranges of two sources are $(5\lambda, 0.5\lambda)$. The input SNR is 5 dB and 200 snapshots are used.

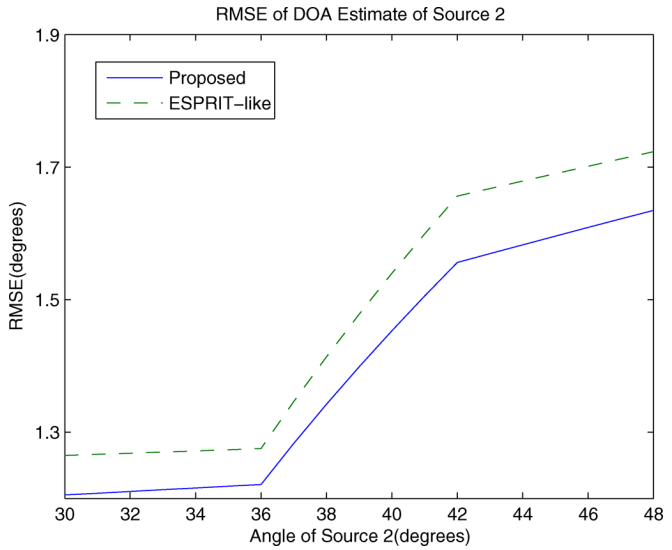

Fig. 7. The RMSE of estimated DOA for source 2 plotted as a function of the DOA of source 2. The DOA of source 1 is fixed at 50° and there are four sensors. The ranges of two sources are $(5\lambda, 0.5\lambda)$. The input SNR is 5 dB and 200 snapshots are used.

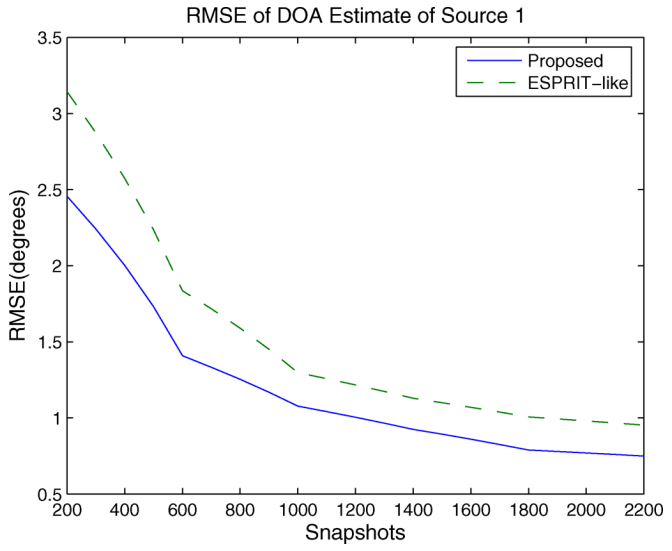

Fig. 8. The RMSE of estimated DOA for source 1 versus input snapshots. The parameters of two sources are $(40°, 5\lambda; 20°, 3.5\lambda)$. There are four sensors and $\mathrm{SNR} = 0$ dB.

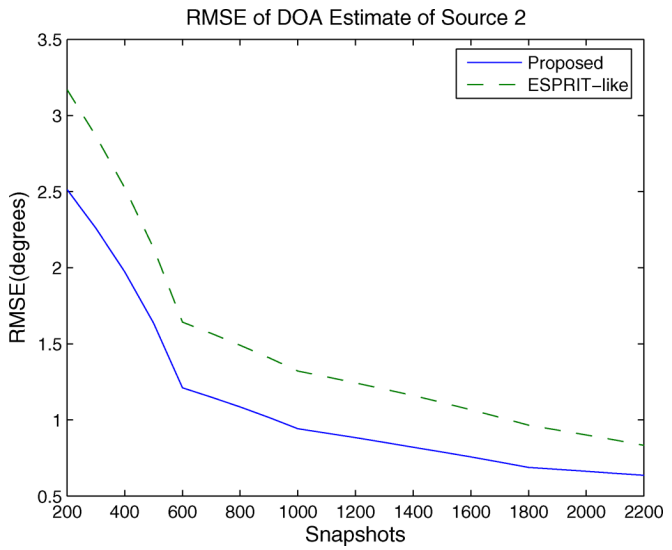

Fig. 9. The RMSE of estimated DOA for source 2 versus input snapshots. The parameters of two sources are $(40°, 5\lambda; 20°, 3.5\lambda)$. There are four sensors and $\mathrm{SNR} = 0$ dB.

DOA estimation for smaller signal-to-noise ratio (SNR) condition although they have almost identical performance at higher SNRs. While from Figs. 4 and 5, we observe that the proposed scheme is superior to [17] for all SNRs in range estimation. It is also seen that the RMSE of the range estimate for the second source, which is closer to the array, is smaller than that of the first source. These phenomena agree with the theoretical analysis in [13], which indicates that the standard deviation of range estimate for the source closer to the array is smaller than that of the source far away from it while the standard deviations of DOA estimates are similar for all sources.

In the second experiment, the performance in angle resolving capability of the proposed method is compared with that of the ESPRIT-like method. The DOA of the first source is fixed at 50° and we vary the DOA of the second source. The ranges of the first and second sources are 5λ and 0.5λ, respectively. The input SNR of the two sources is set to be $\mathrm{SNR} = 5$ dB and 200 samples are taken at each sensor. The RMSEs of the DOA estimates are shown in Figs. 6 and 7 and we can see the superiority of the proposed algorithm for all cases.

In the third experiment, the two sources have the DOA and range parameters as in the first experiment and we vary the number of snapshots used for estimation. The input SNRs of the two sources are fixed at $\mathrm{SNR} = 0$ dB. The RMSEs of the DOA estimates are shown in Figs. 8 and 9 and the superiority of the proposed algorithm for all cases is again observed. It is because the effective aperture size of the proposed method is much larger than that in the ESPRIT-like method.

Finally, Figs. 10 and 11 show that the proposed algorithm can resolve two sources with identical DOA, namely, $\theta_1 = \theta_2 = 20°$, or range, namely, $r_1 = r_2 = 0.5\lambda$. It is noteworthy that the number of sensors $N = 3$ is less than $2P$ with $P = 2$ and thus the ESPRIT-like method cannot be employed in this test.

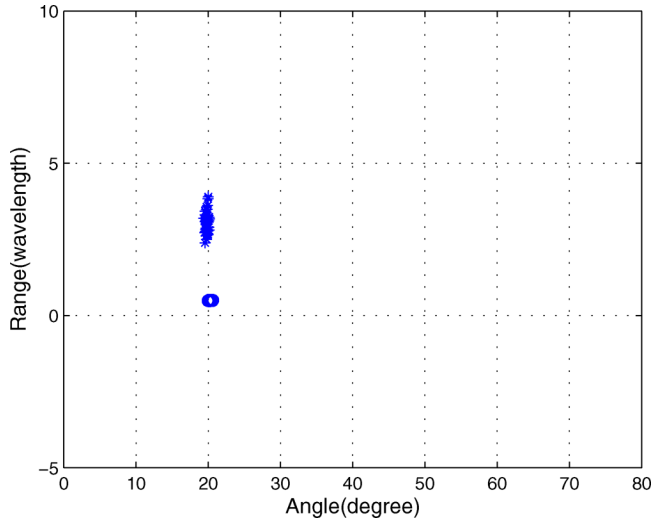

Fig. 10. Simulation results for 50 runs. Two signal sources with identical DOAs are used. The other parameters are $\mathrm{SNR} = 20$ dB, 200 snapshots, and three sensors, actual parameters are $(20°, 5\lambda)$ and $(20°, 0.5\lambda)$, i.e., $\theta_1 = \theta_2$.

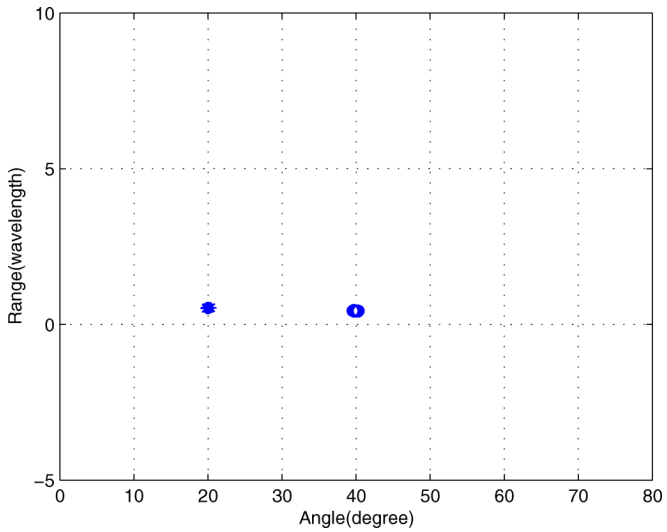

Fig. 11. Simulation results for 50 runs. Two signal sources with identical ranges are used. The other parameters are $\mathrm{SNR} = 20$ dB, 200 snapshots, and three sensors, actual parameters are $(40°, 0.5\lambda)$ and $(20°, 0.5\lambda)$, i.e, $r_1 = r_2$.

V. Conclusion

In this paper, a novel ESPRIT-like method based on cumulants is presented for localization of multiple polarized near-field sources with a polarization sensitive array. The proposed algorithm effectively uses the aperture of array and thus it can estimate the DOAs of $(N-1)$ signal sources using N sensors. The cumulant-based method requires only a simple pair-matching in the case of multiple near-field sources. Furthermore, simulation results demonstrate its effectiveness in both estimation accuracy and resolving capability particularly with a small number of sensors.

Acknowledgment

The authors would like to thank the anonymous reviewers for their careful comments and insightful suggestions, which significantly improved the quality of this paper.

References

[1] H. Krim and M. Viberg, "Two decades of array processing research: The parametric approach," *IEEE Signal Process. Mag.*, vol. 13, no. 4, pp. 67–94, Jul. 1996.

[2] J. H. Kim, I. S. Yang, K. M. Kim, and W. T. Oh, "Passive ranging sonar based on multi-beam towed array," in *Proc. IEEE Oceans*, Sep. 2000, vol. 3, pp. 1495–1499.

[3] A. L. Swindlelhurst and T. Kailath, "Passive direction of arrival and range estimation for near-field sources," in *IEEE Workshop on Spectrum Estimation and Modeling Workshop*, 1988, pp. 123–128.

[4] C. M. Lee, K. S. Yoon, and K. K. Lee, "Efficient algorithm for localising 3-D narrowband multiple sources," *Proc. Inst. Elect. Eng. Radar, Sonar Navig.*, vol. 148, pp. 23–26, Feb. 2001.

[5] Y. D. Huang and M. Barkat, "Near-field multiple sources localization by passive sensor array," *IEEE Trans. Antennas Propag.*, vol. 39, pp. 968–975, Jul. 1991.

[6] R. Jeffers, L. B. Kristine, and H. L. Van Trees, "Broadband passive range estimation using MUSIC," in *Proc. IEEE Int. Conf. Acoust. Speech, Signal Processing*, Orlando, FL, May 2002, pp. 2920–2922.

[7] D. Starer and A. Nehorai, "Path-following algorithm for passive localization of near-field sources," in *Proc. 5th ASSP Workshop on Spectrum Estimation and Modeling*, Oct. 1990, pp. 322–326.

[8] J. H. Lee, C. M. Lee, and K. K. Lee, "A modified path-following algorithm using a known algebraic path," *IEEE Trans. Signal Process.*, vol. 47, pp. 1407–2409, May 1999.

[9] A. J. Weiss and B. Friedlander, "Range and bearing estimation using polynomial rooting," *IEEE J. Ocean. Eng.*, vol. 18, pp. 130–137, Apr. 1993.

[10] R. N. Challa and S. Shamsunder, "Higher-order subspace based algorithms for passive localization of near-field sources," in *Proc. 29th Asilomar Conf. Signals System Computer*, Pacific Grove, CA, Oct. 1995, pp. 777–781.

[11] R. N. Challa and S. Shamsunder, "Passive near-field localization of multiple non-Gaussian sources in 3-D using cumulants," *Signal Processing*, vol. 65, no. 1, pp. 39–53, 1998.

[12] G. Emmanuele and A. M. Karim, "A weighted linear prediction method for near-field source localization," in *Proc. IEEE Int. Conf. Acoust. Speech, Signal Processing*, Orlando, FL, May 2002, pp. 2957–2960.

[13] N. Yuen and B. Friedlander, "Performance analysis of higher- order ESPRIT for localization of near-field sources," *IEEE Trans. Signal Processing*, vol. 46, pp. 709–719, Mar. 1998.

[14] E. R. Ferrara and T. M. Parks, "Direction finding with an array of antennas having diverse polarizations," *IEEE Trans. Antennas Propag.*, vol. 31, pp. 231–236, Mar. 1983.

[15] J. Li and R. J. Compton, "Angle and polarization estimation using ESPRIT with a polarization sensitive array," *IEEE Trans. Antennas Propag.*, vol. 39, no. 9, pp. 1376–1383, 1991.

[16] Y. Hua, "A pencil-MUSIC algorithm for finding two-dimensional angles and polarizations using crossed dipoles," *IEEE Trans. Antennas Propag.*, vol. 41, no. 3, 1993.

[17] B. A. Obeidat, Y. Zhang, and M. G. Amin, "Range and DOA estimation of polarized near-field signals using fourth-order statistics," in *Proc. ICASSP'04*, May 2004, vol. 2, pp. II.97–100.

[18] J. M. Mendel, "Tutorial on high-order statistics in signal processing and system theory: Theoretical results and some applications," *Proc. IEEE*, vol. 79, pp. 278–305, Mar. 1991.

[19] T. H. Liu and J. M. Mendel, "Azimuth and elevation direction finding using arbitrary array geometries," *IEEE Trans. Signal Processing*, vol. 46, 1998.

[20] C. C. Yeh, M. L. Leou, and D. R. Ucci, "Bearing estimations with mutual coupling present," *IEEE Trans. Antennas Propag.*, vol. 37, no. 10, 1989.

[21] T. T. Zhang, H. T. Hui, and Y. L. Lu, "Compensation for mutual coupling effect in the ESPRIT direction finding algorithm by using a more effective method," *IEEE Trans. Antennas Propag.*, vol. 53, no. 4, 2005.

[22] M. Wax and T. Kailath, "Detection of signals by information theoretic criteria," *IEEE Trans. ASSP*, vol. 33, pp. 387–392, 1985.